nature nanotechnology

LETTERS

PUBLISHED ONLINE: 24 APRIL 2017 | DOI: 10.1038/NNANO.2017.52

A STING-activating nanovaccine for cancer immunotherapy

Min Luo[1†], Hua Wang[2†], Zhaohui Wang[1†], Haocheng Cai[2], Zhigang Lu[3], Yang Li[1], Mingjian Du[2], Gang Huang[1], Chensu Wang[1], Xiang Chen[2], Matthew R. Porembka[4], Jayanthi Lea[5], Arthur E. Frankel[6], Yang-Xin Fu[7], Zhijian J. Chen[2,8*] and Jinming Gao[1*]

The generation of tumour-specific T cells is critically important for cancer immunotherapy[1,2]. A major challenge in achieving a robust T-cell response is the spatiotemporal orchestration of antigen cross-presentation in antigen-presenting cells with innate stimulation. Here, we report a minimalist nanovaccine, comprising a simple physical mixture of an antigen and a synthetic polymeric nanoparticle, PC7A NP, which generates a strong cytotoxic T-cell response with low systemic cytokine expression. Mechanistically, the PC7A NP achieves efficient cytosolic delivery of tumour antigens to antigen-presenting cells in draining lymph nodes, leading to increased surface presentation while simultaneously activating type I interferon-stimulated genes. This effect is dependent on stimulator of interferon genes (STING), but not the Toll-like receptor or the mitochondrial antiviral-signalling protein (MAVS) pathway. The nanovaccine led to potent tumour growth inhibition in melanoma, colon cancer and human papilloma virus-E6/E7 tumour models. The combination of the PC7A nanovaccine and an anti-PD-1 antibody showed great synergy, with 100% survival over 60 days in a TC-1 tumour model. Rechallenging of these tumour-free animals with TC-1 cells led to complete inhibition of tumour growth, suggesting the generation of long-term antitumour memory. The STING-activating nanovaccine offers a simple, safe and robust strategy in boosting anti-tumour immunity for cancer immunotherapy.

Cancer immunotherapy using nanoparticle vaccines (nanovaccines) is an emerging area, with recent advances focusing on the co-delivery of antigens and adjuvants[3,4]. Spatiotemporal control of antigen transport to the secondary lymphoid organs, cytosolic delivery and cross-presentation in antigen-presenting cells (APCs) in coordination with innate stimulation are essential to achieve a robust tumour-specific T-cell response. Although nanoparticles (NPs, <50 nm in diameter) can selectively accumulate inside lymph nodes[4,5], few studies had shown their ability to simultaneously promote antigen presentation and stimulate the innate immune response without the incorporation of adjuvants (for example, CpG, poly(I:C)). Recently, our laboratory has developed a library of ultra-pH-sensitive (UPS) NPs (20–50 nm in diameter) that are finely tunable over a broad range of physiological pH (4–7.4)[6]. Once taken up by cells, these NPs can buffer the luminal pH of endocytic organelles at specific pH values[7]. Inspired by 'proton sponge' polymers for cytosolic delivery of biologics[8] and the small NP size for lymph node targeting, we performed an *in vivo* screening of UPS NPs to evaluate their abilities in generating a cytotoxic T lymphocyte (CTL) response. The UPS library consists of copolymers containing tertiary amines with linear or cyclic side chains (Fig. 1a and Supplementary Fig. 1). Ovalbumin (OVA) was used as a model antigen. The OVA loading efficiency was measured to be >75% for different polymer NPs (Supplementary Fig. 2).

The OVA-specific CTL response was quantified by an *in vivo* CTL assay (Fig. 1a). The results show that PC7A NPs allowed the highest OVA-specific splenocyte killings (82%) (Fig. 1b). PC7A NPs yielded an approximately two times stronger CTL response than PC6S1A or poly(ethylpropylamino)ethyl methacrylate (PEPA) NPs with comparable pK_a values (6.9–7.0). In the linear amine series, PEPA had the highest CTL response. These data suggest that both the transition pH (pH 6.9, which targets early endosomal pH) and polymer architecture (the cyclic seven-membered ring of PC7A) are important in inducing a strong CTL response. Conventional PEG-*b*-poly(D,L-lactic acid) (PEG-PLA) micelles had a weak response (4.2%)[9]. OVA-PC7A NPs induced an approximately 20 times higher CTL response when compared with OVA-alum (4.3%) or OVA-lipopolysaccharide (LPS), which stimulate the TLR4 pathway (3.7%)[10], and a 3.6 times higher response than OVA-CpG, which stimulates the TLR9 pathway (23%)[11]. OVA-specific antibody responses from the sera of immunized mice showed that mice vaccinated with PC7A NPs generated titres of OVA-specific IgG1 response comparable to those of alum or LPS (Fig. 1c). PC7A NPs also generated similar titres of OVA-specific IgG2c antibody to those immunized with OVA plus CpG or LPS (Fig. 1d). Altogether, we conclude that PC7A NPs were able to induce robust antigen-specific CTL, Th1 and Th2 responses with comparable or better efficacy than several established adjuvants.

To image NP transport into draining lymph nodes (dLNs), we labelled PC7A copolymer with indocyanine green and quantified the PC7A NP (29 nm in diameter) biodistribution after subcutaneous injection at the tail base. The results show efficient accumulation of PC7A NPs in the peripheral lymph nodes at 24 h (Supplementary Fig. 3a). Other organs did not show significant

[1]Department of Pharmacology, Simmons Comprehensive Cancer Center, University of Texas Southwestern Medical Center, 5323 Harry Hines Boulevard, Dallas, Texas 75390, USA. [2]Department of Molecular Biology, University of Texas Southwestern Medical Center, 5323 Harry Hines Boulevard, Dallas, Texas 75390, USA. [3]Department of Developmental Biology, University of Texas Southwestern Medical Center, 5323 Harry Hines Boulevard, Dallas, Texas 75390, USA. [4]Department of Surgery, University of Texas Southwestern Medical Center, 5323 Harry Hines Boulevard, Dallas, Texas 75390, USA. [5]Department of Obstetrics and Gynecology, University of Texas Southwestern Medical Center, 5323 Harry Hines Boulevard, Dallas, Texas 75390, USA. [6]Department of Internal Medicine, University of Texas Southwestern Medical Center, 5323 Harry Hines Boulevard, Dallas, Texas 75390, USA. [7]Department of Pathology, University of Texas Southwestern Medical Center, 5323 Harry Hines Boulevard, Dallas, Texas 75390, USA. [8]Howard Hughes Medical Institute, University of Texas Southwestern Medical Center, 5323 Harry Hines Boulevard, Dallas, Texas 75390, USA. †These authors contributed equally to this work. *e-mail: jinming.gao@utsouthwestern.edu; zhijian.chen@utsouthwestern.edu

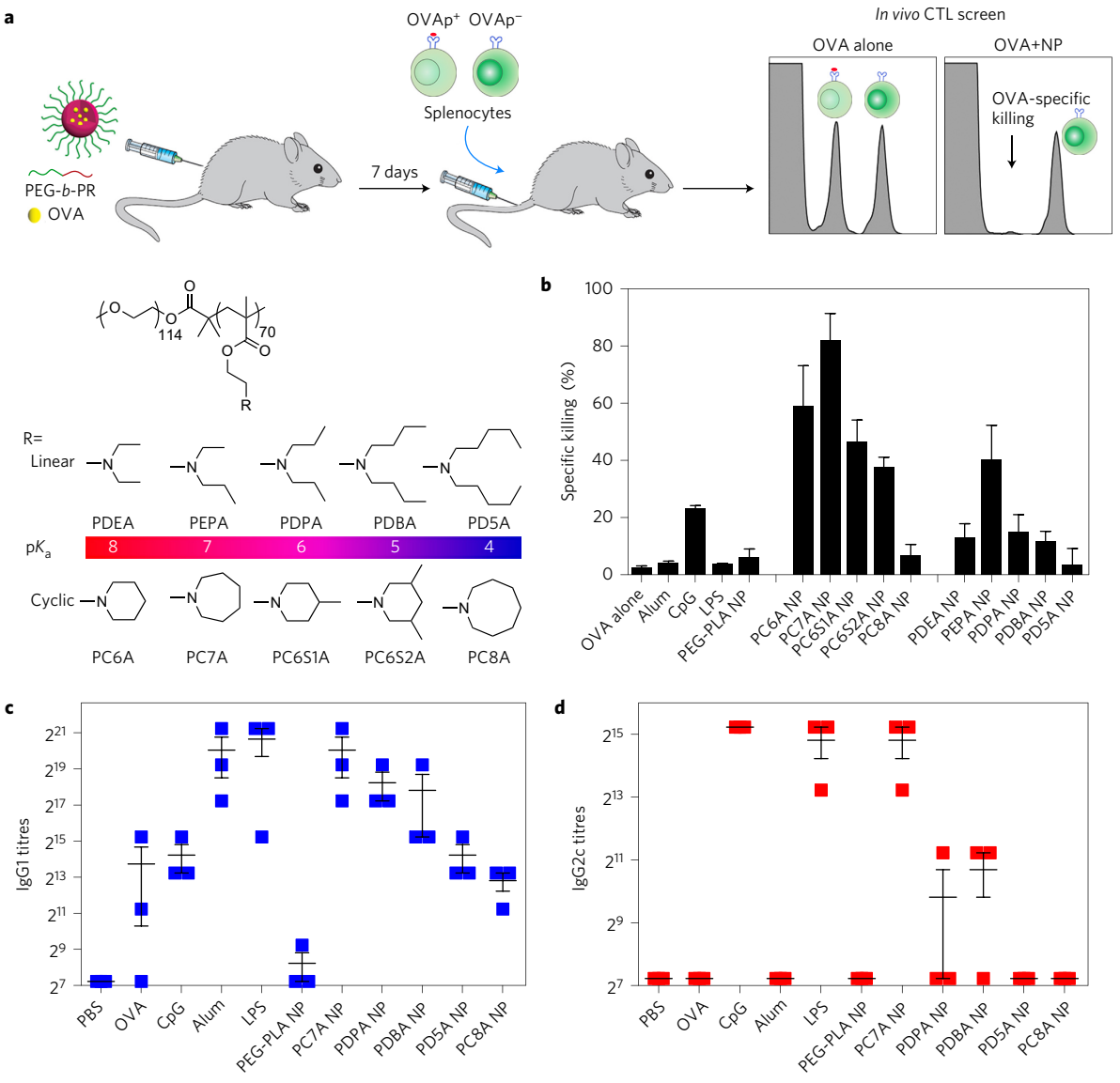

Figure 1 | PC7A NPs induce robust antigen-specific CTL, Th1 and Th2 responses. a, Schematic of the carboxy fluorescein succinimidyl ester (CFSE) method to screen for polymer structures that generate a strong OVA-specific CTL response. OVA was used as a model antigen (10 μg) and loaded into different polymer NPs (30 μg). **b**, Quantitative comparison of OVA-specific CTL responses in different NP groups ($n = 3$ for each group), identifying the PC7A NP as the best candidate. **c**,**d**, OVA-specific productions of IgG1 (**c**) and IgG2c (**d**) as induced by different vaccine groups. PC7A NPs produced broad CTL, Th1 and Th2 responses comparable to or better than the known adjuvants in each category. In **b**–**d**, representative data from three independent experiments are presented as means ± s.e.m.

accumulation. To investigate the ability of PC7A NPs for antigen delivery, we first verified that OVA can be encapsulated in PC7A NPs by a strong fluorescence resonance energy transfer (FRET) effect, and the encapsulation was relatively stable in 5% serum over 24 h (Supplementary Fig. 2). We then used Alexa Fluor 647-labelled OVA with and without PC7A NP encapsulation and collected the dLNs 24 h after subcutaneous injection. Flow cytometry quantified the percentage of OVA-positive cells in $CD8\alpha^+$ and $CD8\alpha^-$ dendritic cells (DCs) and macrophages. All three cell populations showed a significantly higher OVA accumulation by PC7A-mediated delivery over OVA alone (Fig. 2a). LN-resident $CD8\alpha^+$ DC cells are known to be important for induction of the CTL response[12]. The number of OVA-positive $CD8\alpha^+$ DCs increased 29-fold in the OVA-PC7A NP group compared with OVA-only control.

We then investigated the effect of PC7A NPs on cytosolic delivery and cross-presentation of antigens (Fig. 2b)[13]. Incubation of OVA-PC7A NPs with bone-marrow-derived dendritic cells (BMDCs) showed a similar amount of antigen uptake as OVA-PD5A NPs and less than the OVA-only group (Fig. 2c). In contrast, the OVA peptide (SIINFEKL)–MHC-I complex demonstrated a threefold increase in antigen cross-presentation by PC7A NPs over the two control groups (Fig. 2d). Using an *in vitro* OT-I $CD8^+$ T cell priming assay, BMDCs treated with OVA-PC7A NPs dramatically increased the interferon (IFN)-γ secretion of $CD8^+$ T cells isolated from OT-I mice compared with the other control groups (Fig. 2e). This result was further supported by an *in vivo* $CD8^+$ T cell priming assay, where OVA epitope (SIINFEKL)-specific $CD8^+$ T cells showed 15-fold higher proliferation in the OVA-PC7A NPs than in the OVA-only group (Fig. 2f,g). Endosomal disruption for cytosolic delivery was first indicated by a haemolysis assay in red blood cells (RBCs) at different pH values[14]. The results showed that PC7A NPs had no haemolytic effect at pH 7.4, but induced strong haemolysis (~90%) at pH values below 7.0 upon micelle dissociation. PD5A NPs did not show any observable RBC haemolysis in the same pH range (Supplementary Fig. 4a,b). PC7A NPs were able to deliver an increased amount of redox-activatable dye-labelled

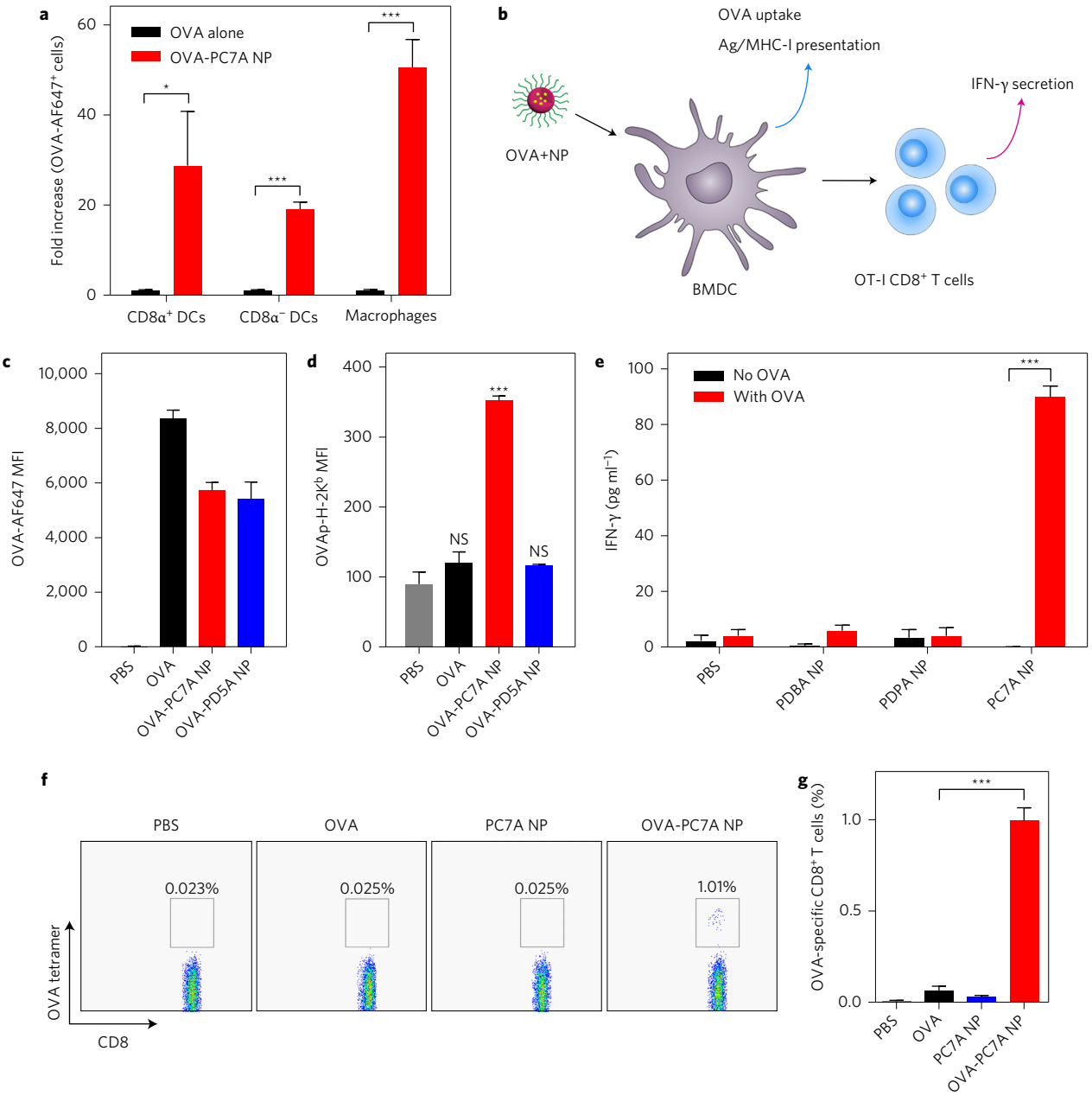

Figure 2 | PC7A NPs improve antigen delivery and cross-presentation in APCs and stimulate CD8 T-cell responses. a, Quantification of OVA-positive cells in three APC subtypes inside lymph nodes 24 h after subcutaneous injection of AF647-OVA-PC7A NPs at the tail base of C57BL/6 mice ($n = 5$). **b**, Schematic of detection of antigen cross-presentation in BMDCs and CD8$^+$ T-cell activation *in vitro*. **c**, Quantification of AF647-OVA uptake in BMDCs by flow cytometry after incubation with AF647-OVA alone, AF647-OVA-PC7A NPs or AF647-OVA-PD5A NPs for 4 h. Mean fluorescence intensity (MFI) of AF647-OVA$^+$ cells in BMDCs was determined ($n = 3$). **d**, Levels of antigen presentation on H-2K^b in BMDCs induced by PC7A or PD5A NPs ($n = 3$). **e**, IFN-γ secretion by OT-I CD8$^+$ T cells after incubating OT-I CD8$^+$ T cells with BMDCs treated with different OVA-NPs ($n = 3$). **f**, Representative flow dot plots of H-2k^b/SIINFEKL tetratmer staining of CD8$^+$ T cells in spleen. **g**, Percentage of OVA (SIINFEKL)-specific CD8$^+$ T cells measured by flow cytometry ($n = 4$). In **a**, **c**–**e** and **g**, representative data from three independent experiments are presented as means ± s.e.m. Statistical significance was calculated by Student's *t*-test: $^{***}P < 0.001$, $^{**}P < 0.01$, $^{*}P < 0.05$. NS, not significant.

OVA into the cell cytosol compared to the PD5A NPs control, as observed by confocal microscopy (Supplementary Fig. 4c)[15].

Co-stimulatory signals (for example, CD80/86) and cytokines are also necessary to induce a strong tumour-specific CTL response[16]. At 24 h post-immunization with OVA-PC7A NPs, inguinal LNs increased in size compared to OVA alone (Supplementary Fig. 3b). The total cell number in the inguinal LNs from OVA-PC7A NP-treated mice increased more than two times compared with controls (Supplementary Fig. 3c). Flow cytometry analysis showed significantly higher expressions of CD86 in different subgroups of APCs from mice treated with OVA-PC7A NPs over three other control groups (Fig. 3a and Supplementary Fig. 3d). Type I IFNs have been shown to boost the effectiveness of the CD8$^+$ T cell response[17,18]. We examined the expressions of IFN-stimulated genes (ISGs) in local tissues[19] over time after subcutaneous injection of PC7A NPs. Poly(I:C) was used as a positive control[20]. Poly(I:C) was able to elicit a higher response in the expression of IRF7 and CXCL10 from 2 to 8 h than PC7A NPs. At 24 h, PC7A NPs produced stronger responses than the poly(I:C) or PD5A NP groups (Fig. 3b,c).

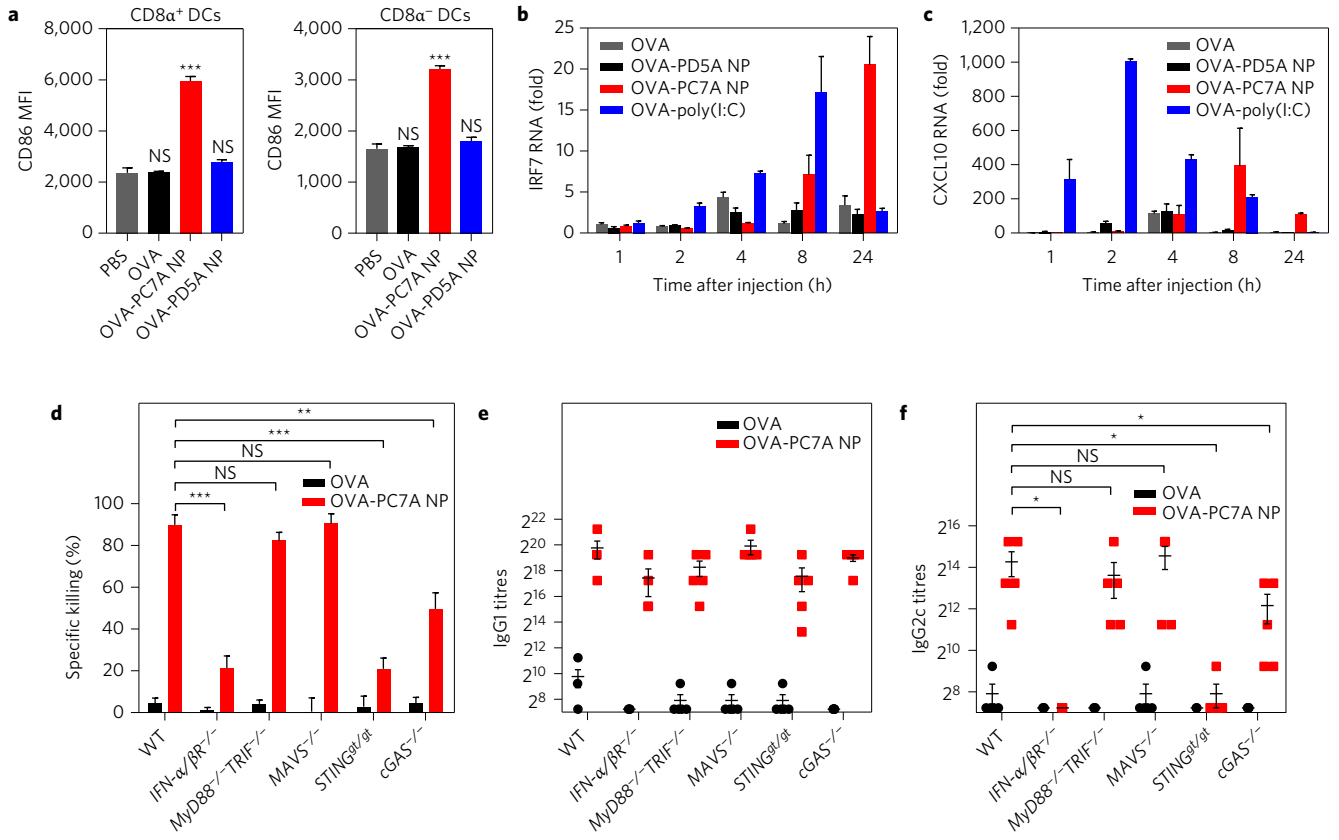

Figure 3 | PC7A NPs activate APCs in draining lymph nodes and stimulate STING-dependent adaptive immune responses. a, Expression of co-stimulator CD86 on CD8α$^+$ and CD8α$^-$ DCs in inguinal lymph nodes 24 h after injection of nanovaccine ($n = 5$ for each group). Data on macrophages and B cells are presented in Supplementary Fig. 3d. **b**,**c**, Measurement of expression levels of interferon-stimulated genes (IRF7 and CXCL10) at the injection site by quantitative polymer chain reaction (qPCR) ($n = 6$). **d**, Quantitative comparison of OVA-specific CTL responses in different knockout mouse groups ($n = 5$ for each group). **e**,**f**, IgG1 (**e**) and IgG2c (**f**) antibody titres in the serum were determined by ELISA ($n = 5$ for each group). Data are presented as means ± s.e.m. Statistical significance was calculated by Student's *t*-test: $^{***}P < 0.001$, $^{**}P < 0.01$, $^{*}P < 0.05$. NS, not significant.

To validate the effect of the type I IFN pathway on the CTL response, we measured the OVA-specific CTL and Th1 response in IFN receptor (*IFN-α/βR*$^{-/-}$) knockout mice. The data show that the majority of the CTL/Th1 response was abolished in *IFN-α/βR*$^{-/-}$ mice compared to wild-type control (Fig. 3d–f), consistent with the ISG expression data. Toll-like receptors (TLR), MAVS and STING are known to activate the type I interferon pathways[17,21]. The immune response in *MyD88*$^{-/-}$*/TRIF*$^{-/-}$, *MAVS*$^{-/-}$ or *STING*$^{gt/gt}$ mice showed that the T-cell response was not dependent on TLR or MAVS, whereas *STING*$^{gt/gt}$ mice almost recapitulated the phenotypes in *IFN-α/βR*$^{-/-}$ mice (Fig. 3d–f). Cyclic GMP-AMP synthase (cGAS) can sense cytosolic DNA and produce cyclic GMP-AMP (cGAMP), which subsequently activates STING, leading to the induction of type I IFNs[22]. Additional studies in *cGAS*$^{-/-}$ mice showed that the CTL response was partially dependent on cGAS. The roles of STING and cGAS in ISG induction were further confirmed by *in vitro* cell culture data using bone-marrow-derived macrophages (BMDMs) and human monocyte THP-1 cells (Supplementary Fig. 5a,b). To evaluate the role of cytosolic DNA in cGAS-dependent STING activation, we transfected DNase I into BMDMs before PC7A treatment[23]. The PC7A-induced ISG level in wild-type BMDMs decreased to almost the same level as in *cGAS*$^{-/-}$ BMDMs (Supplementary Fig. 5c). For cGAS-independent STING activation, we performed a STING pulldown assay using biotin-conjugated PC7A NPs incubated with THP-1 cells. The results show that only PC7A–biotin was able to retain STING, but not PD5A–biotin and PC7A-only (biotin free) controls (Supplementary Fig. 5d). Further pulldown of the purified C-terminal domain (CTD, 139–397 AAs) of STING (Supplementary Fig. 5e) suggests direct binding between STING and PC7A. Isothermal calorimetry analysis showed a dissociation constant (K_d) of 1.3 μM (Supplementary Fig. 5f,g). This interaction is weaker than cGAMP binding to STING ($K_d = 9.6$ nM). Negligible binding was found between PC7A and bovine serum albumin in the negative control. Despite such evidence of a specific interaction between PC7A and STING, further structural and functional studies are required to determine if PC7A can activate STING through direct binding.

To identify which cell populations are responsible for NP uptake and STING activation, Cy5-labelled PC7A polymer was used to quantify NP uptake, and phosphorylated IRF3 (pIRF3) was used to detect the activation of the STING-type I IFN pathway[24]. Flow cytometry analysis showed that in LNs 24 h post-injection, NP$^+$ cells had significantly elevated pIRF3 expressions over NP$^-$ cells (Supplementary Fig. 6a). Furthermore, 87% of NP$^+$ cells expressed a DC cell marker (CD11c$^+$), as corroborated by MHC-II$^+$ expression (Supplementary Fig. 6b). The same analysis was performed on cell suspensions from the injection site (Supplementary Fig. 6c). The data show that CD45$^+$ leukocytes internalized a significantly higher amount of PC7A NPs than CD45$^-$ cells. In the CD45$^-$ cells, we did not observe any significant increase in the pIRF3 levels. In the CD45$^+$ cells, significantly elevated pIRF3 levels were found in the NP$^+$ cells over NP$^-$ cells. About 95% of CD45$^+$NP$^+$ cells showed CD11c$^+$ expression (lower panel in Supplementary Fig. 6d). These data show that APCs, especially DCs, are the major cell population taking up PC7A NPs and subsequently activating the STING-type I IFN pathway.

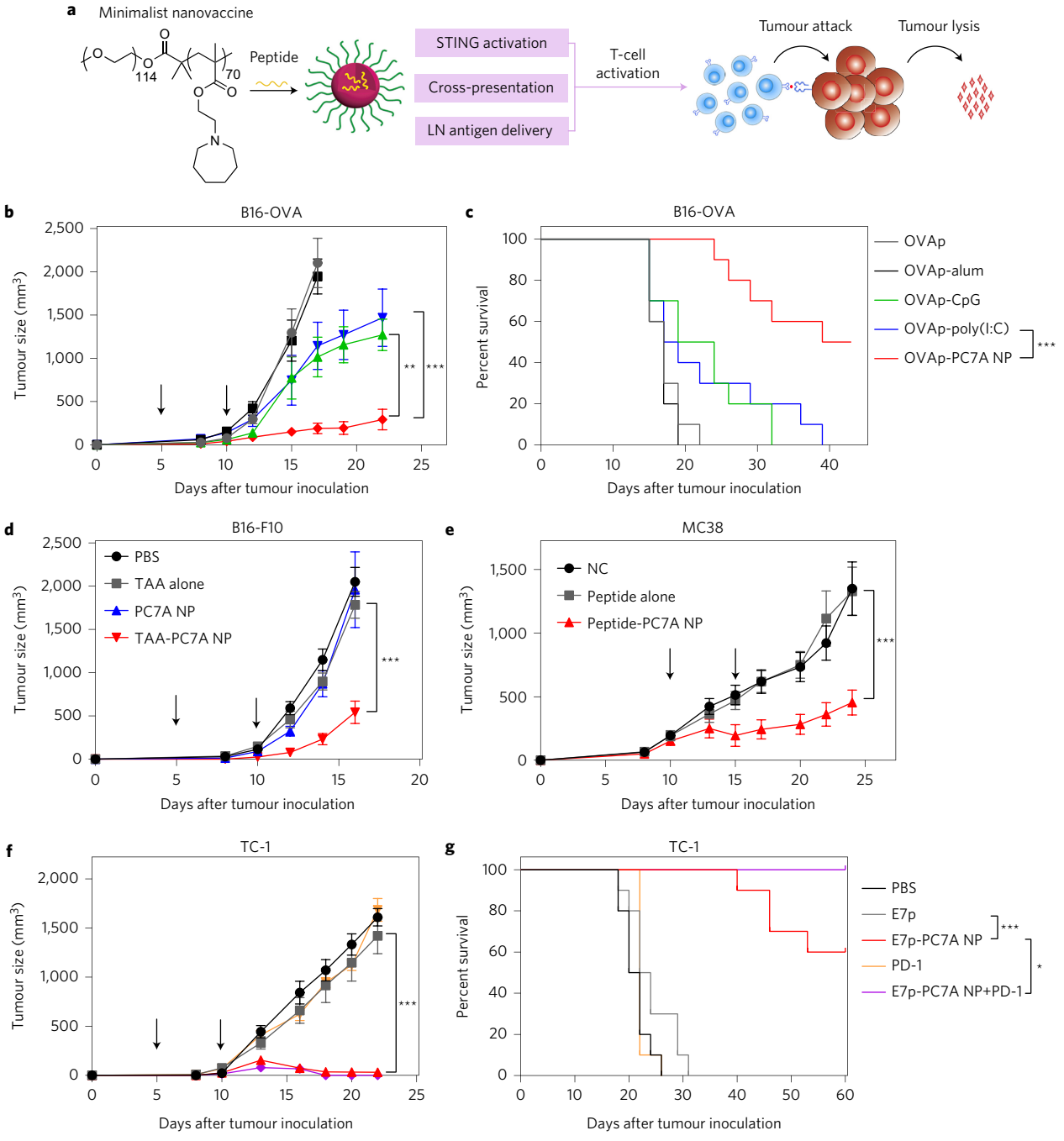

Figure 4 | PC7A nanovaccine inhibits tumour growth and prolongs survival in tumour-bearing mice. a, Schematic of the minimalist design of the PC7A nanovaccine. **b**,**c**, C57BL/6 mice ($n = 10$ per group) inoculated with 1.5×10^5 B16-OVA tumour cells were treated with OVA peptide, PC7A nanovaccine, CpG, poly(I:C) and alum plus peptide (0.5 μg). Tumour growth (**b**) and Kaplan–Meier survival curves (**c**) of tumour-bearing mice are shown. **d**, Tumour growth inhibition study of B16-F10 melanoma. C57BL/6 mice ($n = 10$ per group) inoculated with 1.5×10^5 B16-F10 tumour cells were treated with a cocktail of tumour-associated antigens ($Gp100_{21-41}$, $Trp1_{214-237}$, $Trp2_{173-196}$) in PC7A NPs at specific time points, indicated by arrows. **e**, Tumour growth inhibition study of MC38 colon cancer in C57BL/6 mice. Mice ($n = 10$ per group) inoculated with 1.0×10^6 MC38 tumour cells were treated with a cocktail of neoantigens ($Reps1_{P45A}$, $Adpgk_{R304M}$, $Dpagt1_{V213L}$) in PC7A NPs, and nanovaccine was administered on days 10 and 15 in established tumours (100–200 mm^3). **f**,**g**, In the HPV tumour model, tumour growth inhibition (**f**) and survival data (**g**) in C57BL/6 mice ($n = 10$ per group) were analysed after tumour inoculation with 1.5×10^5 TC-1 tumour cells. In **b** and **d**–**f**, data are presented as means ± s.e.m. Statistical significance was calculated by Student's *t*-test: $^{***}P < 0.001$, $^{**}P < 0.01$, $^{*}P < 0.05$. Statistical significance for survival analysis in **c** and **g** was calculated by the log-rank test: $^{***}P < 0.001$, $^{**}P < 0.01$, $^{*}P < 0.05$.

STING activation has been reported to induce immune regulatory responses such as elevated expressions of indoleamine 2,3-dioxygenase 1 (IDO-1)[25]. We compared the IDO-1 and CXCL10 expression profiles treated with the whole panel of NPs. The results show that the lack of CTL activity by NPs other than PC7A NP is not a result of elevated IDO-1 expression, but rather is due to the lack of STING activation (Supplementary Fig. 5i,j). IDO enzyme activity in mice treated with subcutaneous injections of selected polymers (PC7A, PD5A or PEPA NP, 150 μg, five times the vaccine dose) showed no statistical significance (Supplementary Fig. 5h). The elevated IDO expression by PC7A NPs may warrant future studies of the potential immune checkpoint effect following T-cell activation.

Based on the above characteristics (Fig. 4a), we investigated the antitumour efficacy of PC7A nanovaccine in several tumour models. In the B16-OVA melanoma model, a physical mixture of an antigenic peptide ($OVA_{257-280}$, 0.5 μg) and PC7A NPs (30 μg) was formulated. Different nanovaccine groups were subcutaneously injected 5 days after tumour inoculation, followed by a booster shot 5 days later (Fig. 4b). In the PBS control group, all the animals died within 20 days. $OVA_{257-280}$ alone, PC7A NP alone or $OVA_{257-280}$–PD5A NP groups did not offer any significant tumour growth inhibition or survival benefit over the PBS control (Supplementary Fig. 7a,b). $OVA_{257-280}$–CpG and $OVA_{257-280}$–poly(I:C) groups conferred a minor degree of immune protection (Fig. 4b,c). In contrast, $OVA_{257-280}$–PC7A NPs achieved the maximum therapeutic efficacy, with 50% of animals surviving over 40 days. In B16-F10 melanoma, we used a cocktail of either tumour-associated antigens ($Gp100_{21-41}$, $Trp1_{214-237}$, $Trp2_{173-196}$) or neoantigens ($Obsl1_{T1764M}$, $Kif18b_{K739N}$, $Def8_{R255G}$)[26] in PC7A NPs (0.5 μg for each peptide, 30 μg polymer). PC7A vaccination significantly slowed the growth of B16-F10 tumours over antigen only, PC7A only and non-treated controls (Fig. 4d and Supplementary Fig. 7c). In the colon cancer MC38 model, we selected three tumour neoantigens ($Reps1_{P45A}$, $Adpgk_{R304M}$, $Dpagt1_{V213L}$)[27]. The results show significantly improved tumour growth inhibition (Fig. 4e). Finally, we examined human papilloma virus (HPV) E6/7 TC-1 tumours[28,29]. Using an E7-derived peptide $E7_{43-62}$, 50% of mice were tumour-free 60 days after treatment with $E7_{43-62}$–PC7A NPs (Fig. 4f,g and Supplementary Fig. 8e). The combination of PC7A nanovaccine with an anti-PD-1 antibody showed synergy in both B16-OVA melanoma and TC-1 tumour models (Fig. 4g and Supplementary Fig. 8). In the TC-1 model, 100% of the animals survived for over 60 days and 90% animals were tumour-free (Supplementary Fig. 8e). Both B16-OVA and TC-1 tumour models showed mild PD-L1 expression on tumour cells, while a certain subtype of myeloid cells had high PD-L1 expressions over the isotype control (Supplementary Fig. 8d,f). These data support nanovaccine synergy with anti-PD1 therapy. Meanwhile, anti-PD-1 therapy alone did not lead to a significantly improved antitumour effect in either model, similar to the results of other reports[30,31]. Tumour-free mice were rechallenged with 1×10^6 TC-1 tumour cells 82 days after tumour inoculation. The data show that previously treated, tumour-free mice were resistant to the newly inoculated tumour cells, whereas such tumours grew robustly in naive mice and surgically cured mice (Supplementary Fig. 7e). These results suggest a long-term antitumour response induced by the nanovaccine, which probably activates memory T cells. Analyses of the systemic cytokines/chemokines of mice treated with PC7A NPs (150 μg, five-fold of vaccine dose) showed much lower systemic cytokine levels than with poly(I:C) control (Supplementary Fig. 9). Furthermore, histology analysis of the major organs (for example, liver, spleen, kidney and heart) did not show any observable toxicity in mice treated with repeated injections of PC7A nanovaccine (150 μg, five times the vaccine dose, Supplementary Fig. 10). These data demonstrate the safe and efficacious antitumour immunity from PC7A nanovaccine at a small antigen dose (0.5 μg) and its notable synergy with a checkpoint inhibitor.

In summary, we have discovered a synthetic NP that not only enhances antigen delivery and cross-presentation, but also stimulates the STING pathway to boost antitumour immunity for cancer immunotherapy. The simplicity, robust T cell activation and synergy with checkpoint inhibition make the PC7A nanovaccine an attractive candidate for clinical development. This nanovaccine platform can be rapidly adopted to incorporate many existing tumour-associated antigens as well as a growing number of tumour neoantigens[32,33]. The unique characteristics of the PC7A NPs also allow them to package microbial antigens as vaccines for the prevention and treatment of infectious diseases.

Methods

Methods and any associated references are available in the online version of the paper.

Received 18 May 2016; accepted 3 March 2017;
published online 24 April 2017

References

1. Rosenberg, S. A. & Restifo, N. P. Adoptive cell transfer as personalized immunotherapy for human cancer. *Science* **348,** 62–68 (2015).
2. Tumeh, P. C. *et al.* PD-1 blockade induces responses by inhibiting adaptive immune resistance. *Nature* **515,** 568–571 (2014).
3. Kuai, R., Ochyl, L. J., Bahjat, K. S., Schwendeman, A. & Moon, J. J. Designer vaccine nanodiscs for personalized cancer immunotherapy. *Nat. Mater.* **16,** 489–496 (2017).
4. Liu, H. *et al.* Structure-based programming of lymph-node targeting in molecular vaccines. *Nature* **507,** 519–522 (2014).
5. Reddy, S. T. *et al.* Exploiting lymphatic transport and complement activation in nanoparticle vaccines. *Nat. Biotechnol.* **25,** 1159–1164 (2007).
6. Ma, X. *et al.* Ultra-pH-sensitive nanoprobe library with broad pH tunability and fluorescence emissions. *J. Am. Chem. Soc.* **136,** 11085–11092 (2014).
7. Wang, C. *et al.* A nanobuffer reporter library for fine-scale imaging and perturbation of endocytic organelles. *Nat. Commun.* **6,** 8524 (2015).
8. Boussif, O. *et al.* A versatile vector for gene and oligonucleotide transfer into cells in culture and *in vivo*: polyethylenimine. *Proc. Natl Acad. Sci. USA* **92,** 7297–7301 (1995).
9. Maldonado, R. A. *et al.* Polymeric synthetic nanoparticles for the induction of antigen-specific immunological tolerance. *Proc. Natl Acad. Sci. USA* **112,** E156–E165 (2015).
10. Poltorak, A. *et al.* Defective LPS signaling in C3H/HeJ and C57BL/10ScCr mice: mutations in Tlr4 gene. *Science* **282,** 2085–2088 (1998).
11. Hemmi, H. *et al.* A toll-like receptor recognizes bacterial DNA. *Nature* **408,** 740–745 (2000).
12. Hildner, K. *et al.* Batf3 deficiency reveals a critical role for $CD8\alpha^+$ dendritic cells in cytotoxic T cell immunity. *Science* **322,** 1097–1100 (2008).
13. Heath, W. R. *et al.* Cross-presentation, dendritic cell subsets, and the generation of immunity to cellular antigens. *Immunol. Rev.* **199,** 9–26 (2004).
14. Wilson, J. T. *et al.* pH-responsive nanoparticle vaccines for dual-delivery of antigens and immunostimulatory oligonucleotides. *ACS Nano* **7,** 3912–3925 (2013).
15. Wang, Z. *et al.* A redox-activatable fluorescent sensor for the high-throughput quantification of cytosolic delivery of macromolecules. *Angew. Chem. Int. Ed.* **56,** 1319–1323 (2017).
16. Liechtenstein, T., Dufait, I., Lanna, A., Breckpot, K. & Escors, D. Modulating co-stimulation during antigen presentation to enhance cancer immunotherapy. *Immunol. Endocr. Metab. Agents Med. Chem.* **12,** 224–235 (2012).
17. Zitvogel, L., Galluzzi, L., Kepp, O., Smyth, M. J. & Kroemer, G. Type I interferons in anticancer immunity. *Nat. Rev. Immunol.* **15,** 405–414 (2015).
18. Fuertes, M. B., Woo, S. R., Burnett, B., Fu, Y. X. & Gajewski, T. F. Type I interferon response and innate immune sensing of cancer. *Trends Immunol.* **34,** 67–73 (2013).
19. Trinchieri, G. Type I interferon: friend or foe? *J. Exp. Med.* **207,** 2053–2063 (2010).
20. Alexopoulou, L., Holt, A. C., Medzhitov, R. & Flavell, R. A. Recognition of double-stranded RNA and activation of NF-κB by Toll-like receptor 3. *Nature* **413,** 732–738 (2001).
21. Baccala, R., Hoebe, K., Kono, D. H., Beutler, B. & Theofilopoulos, A. N. TLR-dependent and TLR-independent pathways of type I interferon induction in systemic autoimmunity. *Nat. Med.* **13,** 543–551 (2007).
22. Sun, L., Wu, J., Du, F., Chen, X. & Chen, Z. J. Cyclic GMP-AMP synthase is a cytosolic DNA sensor that activates the type I interferon pathway. *Science* **339,** 786–791 (2013).
23. Carroll, E. C. *et al.* The vaccine adjuvant chitosan promotes cellular immunity via DNA sensor cGAS-STING-dependent induction of type I interferons. *Immunity* **44,** 597–608 (2016).
24. Woo, S. R. *et al.* STING-dependent cytosolic DNA sensing mediates innate immune recognition of immunogenic tumors. *Immunity* **41,** 830–842 (2014).
25. Lemos, H., Huang, L., McGaha, T. L. & Mellor, A. L. Cytosolic DNA sensing via the stimulator of interferon genes adaptor: Yin and Yang of immune responses to DNA. *Eur. J. Immunol.* **44,** 2847–2853 (2014).
26. Kreiter, S. *et al.* Mutant MHC class II epitopes drive therapeutic immune responses to cancer. *Nature* **520,** 692–696 (2015).
27. Yadav, M. *et al.* Predicting immunogenic tumour mutations by combining mass spectrometry and exome sequencing. *Nature* **515,** 572–576 (2014).
28. Sun, Y. Y. *et al.* Local HPV recombinant vaccinia boost following priming with an HPV DNA vaccine enhances local HPV-specific CD8+ T cell mediated tumor control in the genital tract. *Clin. Cancer Res.* **22,** 657–669 (2016).

29. Liu, Z., Zhou, H., Wang, W., Fu, Y. X. & Zhu, M. A novel dendritic cell targeting HPV16 E7 synthetic vaccine in combination with PD-L1 blockade elicits therapeutic antitumor immunity in mice. *Oncoimmunology* **5,** e1147641 (2016).
30. Rice, A. E. *et al.* An HPV-E6/E7 immunotherapy plus PD-1 checkpoint inhibition results in tumor regression and reduction in PD-L1 expression. *Cancer Gene. Ther.* **22,** 454–462 (2015).
31. Holmgaard, R. B., Zamarin, D., Munn, D. H., Wolchok, J. D. & Allison, J. P. Indoleamine 2,3-dioxygenase is a critical resistance mechanism in antitumor T cell immunotherapy targeting CTLA-4. *J. Exp. Med.* **210,** 1389–1402 (2013).
32. Schumacher, T. N. & Schreiber, R. D. Neoantigens in cancer immunotherapy. *Science* **348,** 69–74 (2015).
33. Sharma, P. & Allison, J. P. Immune checkpoint targeting in cancer therapy: toward combination strategies with curative potential. *Cell* **161,** 205–214 (2015).

Acknowledgements

This work was supported by grants from the National Institutes of Health (R01AI093967 to Z.J.C., R01EB013149 and R01CA192221 to J.G.) and the Cancer Prevention and Research Institute of Texas (RP120718-P3 and RP150498 to Z.J.C.). Z.J.C. is an Investigator of the Howard Hughes Medical Institute. M.R.P. is a Dedman Scholar in Clinical Care. Animal imaging work is supported by a UT Southwestern Small Animal Imaging Resource Grant (U24 CA126608) and a Simmons Cancer Center Support Grant (P30 CA142543). The authors thank Z. Zeng for cell culture, Q. Wei for polymer synthesis and T. Zhao for animal imaging. The authors also thank N. Yan for discussions on STING activation, T.C. Wu for providing the TC-1 tumour cells, P. Hwu for the B16-OVA cancer cells, Y. Peng for vaccine safety analysis, S. Tso for ITC experiments and the molecular pathology core of UT Southwestern for tissue toxicity analysis.

Author contributions

M.L. and Z.W. designed and performed the majority of experiments, analysed the data and wrote the first draft of the paper. H.W. made the initial observation of the immune stimulatory activity of PC7A and performed the experiments on CD8 T cell activation by PC7A *in vitro* and *in vivo*. H.C. analysed innate cytokine expression in local tissues and cell lines. Z.L. assisted with the CTL and Th1 experiments. Y.L. and M.D. assisted with the PC7A and STING interaction experiments. G.H. and C.W. assisted with animal efficacy evaluation. X.C. assisted with transgenic mice studies. Y.F. assisted with PD-L1 expression in B16 and TC-1 tumours. M.R.P., J.L. and A.E.F. contributed to experimental designs. Z.J.C. and J.G. supervised all the experiments and revised the final manuscript.

Additional information

Supplementary information is available in the online version of the paper. Reprints and permissions information is available online at www.nature.com/reprints. Publisher's note: Springer Nature remains neutral with regard to jurisdictional claims in published maps and institutional affiliations. Correspondence and requests for materials should be addressed to Z.J.C. and J.G.

Competing financial interests

The authors declare no competing financial interests.

Methods

Materials. Monomers 2-(diethylamino)ethyl methacrylate (DEA-MA) and 2-aminoethyl methacrylate (AMA-MA) were purchased from Polyscience Company. Ovalbumin and $OVA_{257–263}$, CpG oligodeoxynucleotides were purchased from Invivogen, Imject alum was purchased from Thermo Scientific, and LPS and poly(I:C) were purchased from Sigma-Aldrich. $OVA_{257–280}$ (SIINFEKLTEWTSSNV MEERKIKV), $E7_{43–62}$ (GQAEPDRAHYNIVTFCCKCD), $E7_{49–57}$ (RAHYNIVTF), $Gp100_{21–41}$ (VGALEGSRNQDWLGVPRQLVT), $Trp1_{214–237}$ (SHEGPAFLTWH RYHLLQLERDMQE), $Trp2_{173–196}$ (QPQIANCSVYDFFVWLHYYSVRDT), $Obsl1_{T1764M}$ (EGVELCPGNKYEMRRHGTTHSLVIHD), $Kif18b_{K739N}$ (PSKPSF QEFVDWENVSPELNSTDQPFL), $Def8_{R255G}$ (SHCHWNDLAVIPAGVVHN WDFEPRKVS), $Reps1_{P45A}$ (GRVLELFRAAQLANDVVLQIMELCGATR), $Adpgk_{R304M}$ (GIPVHLELASMTNMELMSSIVHQQVFPT) and $Dpagt1_{V213L}$ (EAGQSLVISASII VF NLLELEGDYR) were synthesized by Biomatik. PEG-PLA was purchased from Advanced Polymer Materials. Other solvents and reagents were purchased from Sigma-Aldrich or Fisher Scientific.

Syntheses of methacrylate monomers. Monomers including 2-(ethylpropylamino) ethyl methacrylate (EPA-MA), 2-(dipropylamino)ethyl methacrylate (DPA-MA), 2-(dibutylamino)ethyl methacrylate (DBA-MA), 2-(dipentylamino)ethyl methacrylate (D5A-MA), 2-(pentamethyleneimino)ethyl methacrylate (C6A-MA) and 2-(hexamethyleneimino)ethyl methacrylate (C7A-MA) were synthesized according to previously published methods[34,35]. New monomers including 2-(heptamethyleneimino)ethyl methacrylate (C8A-MA), 2-(4-methylpiperid-ineleneimino)ethyl methacrylate (C6S1A-MA) and 2-(3,5-dimethylpiperi-dineleneimino)ethyl methacrylate (C6S2A-MA) were synthesized following a previously published procedure[35]. The following are the chemical characterizations of the new monomers:

2-(Heptamethyleneimino)ethyl methacrylate (C8A-MA): ^{1}H NMR (TMS, $CDCl_3$, ppm): 6.10 (br, 1H, C*H*H=C(CH_3)-), 5.54 (br, 1H, CH*H*=C(CH_3)-), 4.19 (t, J = 6.1 Hz, 2H, -OCH_2CH_2N-), 2.77 (t, J = 6.1 Hz, 2H, -OCH$_2$CH_2N-), 2.60 (td, 4H, -N(CH_2CH_2CH_2)$_2$CH_2), 1.94 (m, 3H, CH_2=C(CH_3)-), 1.61 (tdd, 2H, -N (CH_2CH_2CH_2)$_2$CH_2), 1.54 (td, 8H, -N(CH_2CH_2CH_2)$_2$CH_2).

2-(4-Methylpiperidineleneimino)ethyl methacrylate (C6S1A-MA): ^{1}H NMR (TMS, $CDCl_3$, ppm): 6.07 (br, 1H, C*H*H=C(CH_3)-), 5.53 (br, 1H, CH*H*=C(CH_3)-), 4.26 (m, 2H, -OCH_2CH_2N-), 2.88 (m, 2H, -OCH$_2$CH_2N-), 2.65 (m, 2H, -N(C*H*HCH$_2$)$_2$CHCH$_3$), 2.04 (tt, 2H, -N(CH*H*CH$_2$)$_2$CHCH$_3$), 1.92 (m, 3H, CH_2=C(CH_3)-), 1.59 (m, 2H, -N(CH$_2$CH*H*)$_2$CHCH$_3$), 1.31 (m, 1H, -C*H*CH$_3$), 1.21 (m, 2H, -N(CH$_2$C*H*H)$_2$CHCH$_3$), 0.89 (d, 3H, -CHCH_3).

2-(3,5-Dimethylpiperidineleneimino)ethyl methacrylate (C6S2A-MA): ^{1}H NMR (TMS, $CDCl_3$, ppm): 6.09 (br, 1H, C*H*H=C(CH_3)-), 5.55 (br, 1H, CH*H*=C (CH_3)-), 4.28 (t, 2H, -OCH_2CH_2N-), 2.85 (ddt, 2H, -OCH$_2$CH_2N-), 2.66 (t, 2H, -N(C*H*HCHCH$_3$)$_2$CH$_2$), 1.94 (m, 3H, CH_2=C(CH_3)-), 1.68 (m, 3H, -N(CH$_2$C*H*CH$_3$)$_2$C*H*H), 1.57 (t, 2H, -N(CH$_2$CHCH$_3$)$_2$CH_2), 0.93 (d, 1H, -N(CH$_2$CHCH$_3$)$_2$CH*H*), 0.84 (d, 3H, -N(CH$_2$CHCH_3)$_2$CH$_2$).

Syntheses of PEG-*b*-PR block copolymers. PEG-*b*-PR copolymers were synthesized by atom transfer radical polymerization (ATRP) following previously reported procedures[36]. PEG-*b*-PDPA is used as an example to illustrate the procedure. First, DPA-MA (7 mmol), PMDETA (0.1 mmol) and MeO-PEG_{114}-Br (0.1 mmol) were dissolved in 2-propanol (2 ml) and DMF (2 ml). After three cycles of freeze–pump–thaw, CuBr (0.1 mmol) was added. The polymerization was carried out at 40 °C for 10 h. The reaction mixture was passed through a neutral Al_2O_3 column, and the residue was dialysed in distilled water and lyophilized. The obtained polymers were characterized by ^{1}H NMR and gel permeation chromatography (GPC).

Syntheses of PEG-*b*-(PR-*r*-dye) block copolymers. AMA-MA was introduced into the PEG-*b*-PR copolymers for the conjugation of dyes according to a similar procedure[34,35]. After synthesis, PEG-*b*-(PR-*r*-AMA) (10 mg) and dye-NHS (1.5 equiv.) were both dissolved in DMF. After overnight reaction, the copolymers were purified by preparative GPC.

Preparation of NPs. Micelles were prepared following a solvent evaporation method[35]. In the example of PEG-*b*-PC7A, copolymer was dissolved in methanol and then added into distilled water under sonication. Methanol was removed using an ultrafiltration tube (M_w = 100 kDa). The NPs were characterized by dynamic light scattering (DLS, Malvern MicroV, He-Ne laser, λ = 632 nm) to determined the hydrodynamic diameter (D_h).

OVA loading and stability studies. OVA loading efficiency inside the NPs was measured by an ultrafiltration method. Briefly, NPs (300 μg ml^{-1}) were mixed with AF647-labelled OVA (100 μg ml^{-1}) for 30 min. Free OVA was removed by ultrafiltration tube with a molecular weight cutoff of 100 kDa. The concentration of free OVA was measured on a Hitachi fluorometer (F-7500 model) with an excitation wavelength at 640 nm. The loading efficiency was calculated according to

$$\text{Loading efficiency} = \frac{\text{Total OVA} - \text{Free OVA}}{\text{Total OVA}} \times 100\%$$

To evaluate the loading stability, OVA-loaded PC7A NPs were incubated in PBS buffer (pH 7.4) containing 5% fetal bovine serum over different periods. Free OVA was separated and determined as described above.

A FRET experiment was carried out to investigate the interactions of polymer and OVA. Typically, Cy3.5-conjugated PC7A (100 μg ml^{-1}) was incubated with AF647-labelled OVA (20 μg ml^{-1}) in PBS buffer (pH 7.4). After 30 min incubation, fluorescence emission spectra were measured on a Hitachi fluorometer (F-7500 model). The samples were excited at 590 nm and the emission spectra were collected from 600 to 750 nm.

Animals and cells. All animal procedures were performed with ethical compliance and approval by the Institutional Animal Care and Use Committee at the University of Texas Southwestern Medical Center. Female C57BL/6 mice (6–8 weeks) were obtained from the UT Southwestern breeding core. *INF-α/βR*$^{-/-}$ mice were provided by D. Farrar (UT Southwestern). *STING*$^{gt/gt}$ mice, *MyD88*$^{-/-}$ mice, *TRIF*$^{-/-}$ mice, C57BL/6$^-$ Tg (TcraTcrb)1100Mjb/J (CD45.2, H-2^b) (OT-I) mice and C57BL/6$^-$ CD45.1 mice were purchased from the Jackson Laboratory. *MyD88*$^{-/-}$/*TRIF*$^{-/-}$ mice were crossed in our laboratory. *cGas*$^{-/-}$ mice were generated as previously described[37]. All strains were maintained on a C57BL/6J background. For each experiment, mice were randomly allocated by blinded investigators to each group. *STING*$^{gt/gt}$ and *cGAS*$^{-/-}$ BMDMs were derived from corresponding knockout mice and then cultured in M-CSF-containing medium for 6–7 days. THP-1 cells were purchased from ATCC, and we established THP-1 cell lines stably expressing shRNA targeting hSTING and hcGAS, as described previously[38]. B16-OVA cells were provided by P. Hwu at MD Anderson Cancer Center, TC-1 cells were provided by T. C. Wu at John Hopkins University, and MC38 cells were purchased from ATCC. All cell lines were routinely tested using a mycoplasma contamination kit (R&D). Cells were cultured in complete medium (DMEM, 10% fetal bovine serum, 100 U ml^{-1} penicillin G sodium and 100 μg ml^{-1} streptomycin (Pen/Strep), MEM non-essential amino acids (all from Invitrogen) and 20 μM β-mercaptoethanol (β-ME)) at 37 °C in 5% CO_2 and the normal level of O_2.

***In vivo* cytotoxicity killing assay.** Groups of C57BL/6 mice were injected (10 μg OVA plus 30 μg NPs or other adjuvants with the same dose) subcutaneously at the tail base of C57BL/6 mice. Imject alum (4 mg per mouse, 50 μl:50 μl mixture with the antigen solution) was used by volume ratio, as recommended by the manufacturer. One week later, naive C57BL/6 mice were killed, and splenocytes were collected. Half of the splenocytes were pulsed with $OVA_{257–263}$ or $E7_{49–57}$ peptides for 2 h in complete medium at 37 °C. The unpulsed and peptide-pulsed cells were labelled with 0.5 or 0.05 μM carboxyfluorescein succinimidyl ester (CFSE), respectively, in serum-free medium for 15 min. Equal numbers (1×10^7) of CFSE^{low} (OVA pulsed) and CFSE^{high} (unpulsed) cells were mixed together and injected intravenously into the immunized mice. After 16 h, blood from treated mice was collected and subjected to flow cytometry analysis. The numbers of CFSE^{high} and CFSE^{low} cells were determined and used to calculate the percentage of OVA peptide-pulsed target cell killing. Specific killing was defined as

$$\text{Percentage of specific lysis} = [1 - \text{non-transferred control ratio}/\text{experimental ratio}] \times 100$$

ELISA assay. For antibody detection, groups of C57BL/6 mice were immunized with different vaccines on days 0 and 14. On day 21, 50 μl blood was drawn from the tail vein, and levels of antigen-specific IgG1 and IgG2c in the serum were measured by ELISA. For ELISA assay, flat-bottomed 96-well plates (Nunc) were precoated with OVA protein at a concentration of 0.5 μg protein per well in 50 mM carbonate buffer (pH 9.6) at 4 °C overnight, which were then blocked with 5% glycine. Antisera obtained from immunized animals were serially diluted from 10^2 to 10^6 in PBS-0.05% Tween (PBS-T), pH 7.4, and were added to the wells and incubated at 37 °C for 1 h. Horseradish peroxidase (HRP) conjugated goat anti-mouse IgG1 and IgG2c (Abcam) were used at a dilution of 1:10,000 in PBS-T–1% BSA for labelling. After adding the HRP substrates, optical densities were determined at a wavelength of 450 nm in an ELISA plate reader (Bio-Rad).

Lymph node imaging assay. To investigate whether NPs can accumulate in the draining lymph nodes, we labelled the PC7A copolymer with indocyanine green (ICG) ($\lambda_{ex}/\lambda_{em}$ = 800/820 nm). ICG-encoded PC7A NPs (30 μg per mice) were injected subcutaneously into the tail base of C57BL/6 mice. NP distribution was imaged using a clinical camera (SPY Elite). Animals were killed at 24 h after injection of NPs, and major organs and inguinal and axillary LNs were excised and imaged.

***In vivo* cell uptake assay.** For antigen delivery assay, subcutaneous injections at the tail base of C57BL/6 mice were performed with PBS alone, OVA-AF647, or NP plus OVA-AF647 treatments. At 24 h post injection, mice were killed and inguinal lymph nodes were removed, teased with 26 gauge needles and then passed through a 70 μm cell strainer (BD) to recover a cell suspension. The lymph node cell suspension was stained with propidium iodide (PI) and anti-CD11c-FITC, anti-CD11b-pacific blue, anti-B220-APC-Cy7 and anti-CD8a-PE-Cy7. Four major APC populations (CD8α$^+$

DC cells ($CD11c^+$ $CD11b^-$ $B220^-$ $CD8\alpha^+$), $CD8\alpha^-$ DC cells ($CD11c^+$ $CD8\alpha^-$), macrophage cells ($CD11b^+$ $CD11c^-$ $B220^-$) and B cells ($B220^+$ $CD11c^-$)) were analysed for the OVA-AF647 positive cells. APC maturation was measured by staining with anti-CD86-PE.

For NP uptake and STING activation assay, subcutaneous injections at the tail base of C57BL/6 mice were carried out with PBS alone or PC7A-Cy5 (30 μg) treatments. At 24 h post injection, mice were killed, and inguinal lymph nodes and subcutaneous tissue were removed and digested in collagenase IV (Sigma-Aldrich) solution for 25 min at 37 °C. Tissue was then passed through a 70 μm cell strainer (BD) to recover a cell suspension. All the cell suspensions were stained with PI and anti-CD11c-FITC, anti-MHCII-BV605 and anti-CD45.2-Apc-Cy7. For intracellular pIRF3 staining, cells were permeabilized by a fixation/permeabilization kit (BD cat. no. 554714). After blocking with mouse serum, cells were stained with pIRF3 antibody (Cell Signaling, cat. no. 4947) and subsequently stained with anti-rabbit IgG-PE secondary antibody (Biolegend). Flow cytometry (LSRII, BD) was performed on stained cell suspensions and analysed with FlowJo software (Tree Star).

***In vitro* cell uptake and cross-presentation assay.** BMDCs were generated by culturing bone marrow cells flushed from the femurs of C57BL/6J mice in DC medium: DMEM supplemented with 10% FBS, Pen/Strep, sodium pyruvate and 20 ng ml^{-1} GM-CSF. The medium was half replaced every 2 days. Non-adherent and loosely adherent immature DCs were collected on day 6 and phenotyped by determining the expression of CD11c (routinely 60–80% $CD11c^+$). OVA-AF647 (2 μg ml^-) or a mixture of OVA-AF647 and different NPs (50 μg ml^{-1}) was incubated with murine BMDCs at 37 °C for 4 h and quantified using the mean fluorescence intensity (MFI) of cells by flow cytometry analysis. For the cross-presentation assay, BMDCs were incubated with OVA alone or a mixture of OVA and different NPs at 37 °C for 18–20 h, then the $OVA_{257-267}$ presented on the MHC-I on the cell surface was detected by monoclonal antibody 25 mAb-D1.16, an antibody that specifically recognizes OVA peptide SIINFEKL bound to $H\text{-}2K^b$.

***In vitro* $CD8^+$ T cell priming assay.** To evaluate antigen presentation by OVA-NP-pulsed BMDCs, IFN-γ secretion by primed OT-I T cells was used to quantify $CD8^+$ T-cell activation. Briefly, BMDCs were incubated with 3 μg ml^{-1} OVA alone or a mixture of OVA with different NPs (50 μg ml^{-1}) at 37 °C for 18 h. $CD8^+$ T lymphocytes from OT-I mice were selected by magnetic separation (MACS system; Miltenyi Biotec) according to the manufacturer's instructions. The purity of $CD8^+$ T lymphocytes was >95%. $CD8^+$ T cells were plated at 2×10^5 cells per well in 96-well plates (Costar, Corning) in RPMI medium containing 10% FCS and 2×10^5 unpulsed or antigen-pulsed BMDCs, which were added for 24 h. Cell culture supernatants were collected and analysed for cytokine content using a mouse TH1/TH2 9-Plex Ultra-sensitive Kit (Meso Scale Discovery). Samples were run in triplicate.

***In vivo* $CD8^+$ T cell priming assay.** Spleens were collected from B6 $CD45.2^+$ OT-I mice, and $CD8^+$ T cells from cell suspensions were isolated by magnetic bead separation on a MACS column. A total of 5×10^4 OT-1 $CD8^+$ T cells were transferred into B6 $CD45.1^+$ mice via intravenous injection and allowed to acclimate for 1 day before immunization. After 1 day, groups of $CD45.1^+$ mice were immunized subcutaneously with PBS alone, OVA(10 μg) or NP (30 μg) plus OVA at the tail base. One week later, spleens were collected and dispersed into single-cell suspensions, stained with anti-CD8-PE-cy7, APC-conjugated H-2Kb/OVA (SIINFEKL) tetramer (NIH) for flow cytometry analysis.

Haemolysis assay. The capacity of polymers to promote pH-dependent disruption of lipid bilayer membranes was assessed by a RBC haemolysis assay as previously described[14]. Polymers were incubated for 1 h at 37 °C in the presence of mouse erythrocytes at 20 μg ml^{-1} in 100 mM sodium phosphate buffer (supplemented with 150 mM NaCl) in the pH range of the endosomal processing pathway (7.4, 7.2, 7.0, 6.8, 6.6 and 6.4). The extent of cell lysis (that is, haemolytic activity) was determined spectrophotometrically by measuring the amount of haemoglobin released (A541 nm). Haemolytic activity was normalized to 100% lysis control (1% Triton X-100 treated RBCs). Samples were run in triplicate.

Flow cytometry. Antibodies were purchased from Biolegend. The following primary antibodies were used: anti-CD16/CD32 (Biolegend, cat. no. 101301, clone 93), anti-CD8-PE-cy7 (Biolegend, cat. no. 100721, clone 53–6.7), anti-CD11c-FITC (Biolegend, cat. no. 117305, clone N418) and anti-CD11b-pacific blue (Biolegend, cat. no. 101223, clone M1/70), anti-B220-APC-cy7 (Biolegend, cat. no. 103223, clone RA3–6B2), anti-CD86-PE (Biolegend, cat. no. 105007, clone GL-1), anti-$H\text{-}2K^b$ bound to SIINFEKL-APC (Biolegend, cat. no. 141605, clone 25-D1.16), anti-CD45.2-APC (Biolegend, cat. no. 109814, clone 104), anti-CD45.2-APCcy7 (Biolegend, cat. no. 109823, clone 104), anti-PD-L1-PE (Biolegend, cat. no. 124307, clone 10F.9G2), isotype control-PE (Biolegend, cat. no. 400607, clone RTK4530), anti-F4/80-PE/cy7 (Biolegend, cat. no. 123113, clone BM8), anti-Gr-1-FITC (Biolegend, cat. no. 108419, clone RB608C5), anti-MHCII-BV605 (Biolegend, cat. no. 107639, clone M5/114.15.2) and anti-rabbit IgG-PE (Biolegend, cat. no. 406421, clone poly4064). Flow data were acquired on a BD LSR II flow cytometer and analysed using FlowJo software.

Quantitative reverse transcription polymerase chain reaction (qRT-PCR). Subcutaneous tissues were taken at indicated time points after injection with OVA-PC7A NPs (10 μg OVA, 150 μg PC7A) or the same dose of different adjuvants. To obtain BMDMs, ~1×10^7 bone marrow cells were cultured in DMEM containing 10% FBS, antibiotics and conditioned medium from L929 cell culture. After 6 to 7 days, mature macrophages were collected and cultured on 12-well plates for experiments[5]. Total RNAs were extracted by TRIzol (Invitrogen) from cells or tissues, according to the manufacturer's instructions. qRT–PCR was performed as previously described[37,38]. Samples were run in triplicate. The following primers were used for qRT–PCR.

mIRF7: ATGCACAGATCTTCAAGGCCTGGGC;
GTGCTGTGGAGTGCACAGCGGAAGT
mCXCL10: GCCGTCATTTTCTGCCTCA; CGTCCTTGCGAGAGGGATC
mIDO-1: CGGACTGAGAGGACACAGGTTAC;
ACACATACGCCATGGTGATGTAC
mRPL19: AAATCGCCAATGCCAACTC; TCTTCCCTATGCCCATATGC
hCXCL10: TGGCATTCAAGGAGTACCTC; TTGTAGCAATGATCTCAACACG
hIDO-1: GCCAGCTTCGAGAAAGAGTTG; ATCCCAGAACTAGACGTGCAA
hGAPDH: ATGACATCAAGAAGGTGGTG; CATACCAGGAAATGAGCTTG

DNase I transfection. BMDMs were transfected with 5 μg DNase I (Roche) by transfection reagent DOTAP (Roche) according to the manufacturer's instructions. After incubating the cells with DOTAP-DNase I or DOTAP alone for 1 h, cells were washed to remove excess transfection reagent and enzyme and were then incubated with PC7A at 400 μg ml^{-1} for 9 h. CXCL10 was measured by RT–PCR.

STING pulldown assay. To investigate the STING interaction with PC7A copolymer, we labelled the PC7A copolymer with biotin (2–3 biotins per polymer chain). For THP-1 cell pulldown assay, PC7A–biotin (200 μg ml^{-1}) was incubated with THP-1 cells for 8 h, then cells were collected and lysed in RIPA buffer (Sigma R0278). Lysates were precipitated with streptavidin-modified Dynabeads (BD 557812). Samples were analysed using SDS–PAGE and western blots by rabbit anti-STING antibody (Cell Signaling, cat. no. 13647). For STING protein pulldown assay, human STING CTD (139–379) expression and purification has been described before[39]; PC7A-biotin (50 μg ml^{-1}) was incubated with STING CTD (1 μg ml^{-1}) for 3 h in PBS (pH 6.8), and PEPA–biotin in PBS (pH 6.8) and PD5A–biotin in PBS (pH 4.4) with the same concentration were used as control groups and then precipitated with streptavidin-modified Dynabeads. Samples were analysed using SDS–PAGE and western blots.

Isothermal titration calorimetry (ITC). ITC was used to measure the binding affinities between STING CTD and PC7A polymers or cGAMP using a VP-ITC microcalorimeter (GE Healthcare), and ITC of PC7A–BSA was used as negative control. Titrations were performed at 20 μC in buffer containing 25 mM HEPES (pH 6.8) and 150 mM NaCl. Thirty-two injections were performed with 4 min spacing time. The titration traces were integrated by NITPIC, and the curves were fitted by SEDFIT[39]. The figures were prepared using GUSSI (http://biophysics.swmed.edu/MBR/software.html).

IDO enzyme activity assay in tissues. Bacterial pDNA (pEGFPN1, Clontech) was prepared using an endotoxin-free kit (Qiagen). Mice were intravenously injected with 30 μg pDNA mixed with *in vivo*-jetPEI (Polyplus-transfection, N:P = 8) or were injected s.c. with NPs (150 μg, five times the vaccine dose). IDO activity was measured as described in previous reports[40,41]. Enzyme activity was expressed as the product content per hour per gram of tissue protein.

Immunization and tumour therapy experiments. Six- to eight-week-old mice ($n = 10$ for each group) were injected subcutaneously with B16-OVA or B16F10 melanoma cells (1.5×10^5), TC-1 cells (1.5×10^5) or MC38 cells (5×10^5) into the right flank of mice. Animals were immunized by subcutaneous injection into the tail base of antigen–polymer NPs (0.5 μg per antigen peptide, PC7A NP 30 μg) or the same dose of different adjuvants as described in the main text. Alternatively, at days 3, 6, 9 and 12, some groups were intraperitoneally injected with 200 μg checkpoint inhibitors (anti-mPD-1, BioXcell, BE0146) for comparison or synergy evaluation. Tumour growth was subsequently measured twice a week using a digital caliper and calculated as $0.5 \times \text{length} \times \text{width}^2$ by blinded investigators. Mice were killed when the tumour volumes reached 1,500 mm^3 (the end point of tumour detection is two times the longest survival time (LST) of the control group, so about 40 days for the melanoma tumour model and about 60 days for TC-1 and MC38 tumour models).

For PD-L1 expression analyses, tumour tissues were digested by 1 mg ml^{-1} collagenase IV (Sigma-Aldrich) and 0.2 mg ml^{-1} DNase I (Sigma-Aldrich) for 45 min at 37 °C. Cells were then stained with antibodies against PD-L1, CD11b, Gr-1, F4/80, CD11c and CD45 (Biolegend).

Statistical analysis. Based on pilot immunization and tumour treatment studies, we used group sizes of three to six animals per group for immunogenicity measurements and ten animals per group for tumour therapy experiments. Statistical analysis was performed using Microsoft Excel and Prism 5.0 (GraphPad). Data are expressed as

means ± s.e.m. Data were analysed by Student's *t*-test. A variance similarity test (*f*-test) was performed before the *t*-test. All *t*-tests were one-tailed and unpaired, and were considered statistically significant if $P < 0.05$ ($^{*}P < 0.05$, $^{**}P < 0.01$, $^{***}P < 0.001$, unless otherwise indicated). The survival rates of the two groups were analysed using a log-rank test and were considered statistically significant if $P < 0.05$.

Data availability. The data sets generated and/or analysed during the study are available from the corresponding authors upon request.

References

34. Zhou, K. *et al.* Tunable, ultrasensitive pH-responsive nanoparticles targeting specific endocytic organelles in living cells. *Angew. Chem. Int. Ed.* **50,** 6109–6114 (2011).
35. Zhou, K. *et al.* Multicolored pH-tunable and activatable fluorescence nanoplatform responsive to physiologic pH stimuli. *J. Am. Chem. Soc.* **134,** 7803–7811 (2012).
36. Tsarevsky, N. V. & Matyjaszewski, K. 'Green' atom transfer radical polymerization: from process design to preparation of well-defined environmentally friendly polymeric materials. *Chem. Rev.* **107,** 2270–2299 (2007).
37. Li, X. D. *et al.* Pivotal roles of cGAS-cGAMP signaling in antiviral defense and immune adjuvant effects. *Science* **341,** 1390–1394 (2013).
38. Collins, A. C. *et al.* Cyclic GMP-AMP synthase is an innate immune DNA sensor for *Mycobacterium tuberculosis*. *Cell Host Microbe.* **17,** 820–828 (2015).
39. Zhang, X. *et al.* Cyclic GMP-AMP containing mixed phosphodiester linkages is an endogenous high-affinity ligand for STING. *Mol. Cell* **51,** 226–235 (2013).
40. Huang, L. *et al.* Engineering DNA nanoparticles as immunomodulatory reagents that activate regulatory T cells. *J. Immunol.* **188,** 4913–4920 (2012).
41. Hoshi, M. *et al.* The absence of IDO upregulates type I IFN production, resulting in suppression of viral replication in the retrovirus-infected mouse. *J. Immunol.* **185,** 3305–3312 (2010).